Heliyon 9 (2023) e21014

Contents lists available at ScienceDirect

Heliyon

journal homepage: www.cell.com/heliyon

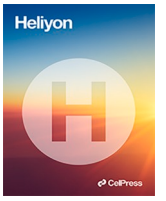

New benzisoxazole derivative: A potential corrosion inhibitor for mild steel in 0.5 M hydrochloric acid medium -insights from electrochemical and density functional theory studies

Preethi Kumari P [a], Anusha G [a], J.N Cheerlin Mishma [b], Rajeev K. Sinha [c], Aishwarya S. Suvarna [d], Santosh L. Gaonkar [a,*]

[a] Department of Chemistry, Manipal Institute of Technology, Manipal Academy of Higher Education, Manipal, 576104, India
[b] Department of Physics, Women's Christian College, Nagercoil, Tamil Nadu, India
[c] Department of Physics, Birla Institute of Technology, Mesra, Ranchi - 835215, Jharkhand, India
[d] Department of Chemistry, National Institute of Technology Karnataka, 575025, India

ARTICLE INFO

Keywords:
Benzisoxazole derivative
corrosion
DFT
Adsorption
Electrochemical measurement

ABSTRACT

6-fluoro-3-(4-piperidinyl)-1,2-benzisoxazole. HCl (FPBH), a substituted benzisoxazole derivative, was prepared from isonipecotic acid and characterized using various spectroscopic techniques. Using electrochemical examinations such as potentiodynamic polarisation (PDP) and electrochemical impedance spectroscopic (EIS) technique, the corrosion mitigation capabilities of this compound for mild steel (MS) in 0.5 M HCl medium were investigated. Theoretical studies were performed using quantum chemical calculations and density functional theory (DFT). PDP results exhibited the mixed-type behavior of FPBH and showed a maximum efficiency of 94.5 % at 1×10^{-3} M. The development of a protective adsorbed layer of FPBH decreases the corrosion current density (i_{corr}) and corrosion rate (CR). The EIS technique revealed that the rise in the charge transfer resistance (R_{ct}) values and reduction in the thickness of the double-layer capacitance (C_{dl}) reflected the drop in corrosion rate. The adsorption of FPBH took place through physisorption by conforming Langmuir's isotherm. The DFT method was performed on the optimized structure of FPBH to get additional evidence on the action mode of FPBH with the metal surface.

1. Introduction

The study of corrosion is no longer a concern only for metallurgists and chemists; it has universal importance for a better understanding of the process and managing it profoundly. The major concern would be to increase the life of the metal and reduce damage. Mild steel (MS) is the foremost commonly spread metallic element on the Earth's crust. It is one of the industry's most widely used iron-based alloys in different metal structures and equipment owing to its unique physicochemical properties. In addition, metallic flow components especially steel pipeline systems are frequently employed in oil and gas firms to transfer fluids. When in contact with numerous types of fluids, the corrosion phenomena drastically deteriorate the lifespan of pipeline constructions and create a significant impact on the global economy [1,2]. Preventing steel corrosion has played an essential role in various chemical and petrochemical processing industries that employ steel material in different applications [3]. Hydrochloric acid is typically utilized in

* Corresponding author.
E-mail address: sl.gaonkar@manipal.edu (S.L. Gaonkar).

https://doi.org/10.1016/j.heliyon.2023.e21014
Received 4 May 2023; Received in revised form 12 October 2023; Accepted 12 October 2023
Available online 17 October 2023

the pickling process since ferrous chloride generated on the surface is extremely soluble in water and does not cause smudge formation on the surface. The least polarising effect is produced by the high rate of solubility of chloride salts, does not hamper the rate of reaction. The acid cleaning of MS is considered one of the crucial processing steps to take away the oxide layer formed during the annealing and hot rolling process, but it could lead to its deterioration [4]. Corrosion inhibitors play a significant role in reducing metallic loss and material failure in various industrial sectors [5,6].

Organic compounds have been investigated as potential corrosion inhibitors for the last several years. The molecules holding hetero atoms, aromatic rings, unsaturated bonds, and planar structures with large surface areas contribute immensely towards corrosion control by physicochemical interaction with the metal surfaces [7–10].

The potential inhibitors are likely to perform under various conditions, such as their stability, solubility in an aqueous medium and over the wide range of temperatures used, etc. Hence, the selection of inhibitor compounds seeks high importance before its practical application. Though many organic inhibitors containing hetero atoms can be used as corrosion inhibitors, the inhibition performance decreases due to their solubility issue in an aqueous solution. Hence, searching for an effective water-soluble corrosion inhibitor is challenging and highly required.

Substituted 1,2-benzisoxazoles are an important class of heterocycles and a widely explored class of compounds in the last few decades, primarily due to their diverse medicinal properties [11]. Extensive research work was carried out on the synthesis of 1,2-benzisoxazole heterocycles. Isoxazole analogs also emerged as potential corrosion inhibitors among azole-class compounds. They are expected to reinforce the adsorption in highly corrosive conditions and propensity to bind with metallic surfaces [12].

FPBH is an intermediate in the preparation of many pharmaceutically useful compounds [13]. In this context, such structures are gaining interest and were investigated for their medicinal applications. Recently, a few number of isoxazole derivatives were studied for their corrosion-inhibitory properties against several metals and alloys [14,15]. However, isoxazoles combined with other heterocycles are not explored as corrosion inhibitors. Therefore, a combination of electron-rich piperidine and isoxazole derivative looks attractive for corrosion studies. Prompted by these and continuing our work on synthesizing heterocyclic compounds [16] here, we report the corrosion inhibition studies of 5 and 6-membered heterocyclic hybrid compound FPBH on MS in an acidic environment.

2. Experimental

2.1. Material and corrosive medium

The commercially available MS with the compositions C (0.04), Si (0.18), Mn (0.77), S (0.01), Cr (0.01), Ni (0.006), and Mo (0.019) were employed for the corrosion study. The rod-shaped coupons of MS samples are embedded with epoxy resin with an uncovered surface area of 1 cm^2. The freshly polished and cleaned MS sample was then made to contact with deareated 0.5 M HCl to measure the rate of corrosion without and with an inhibitor.

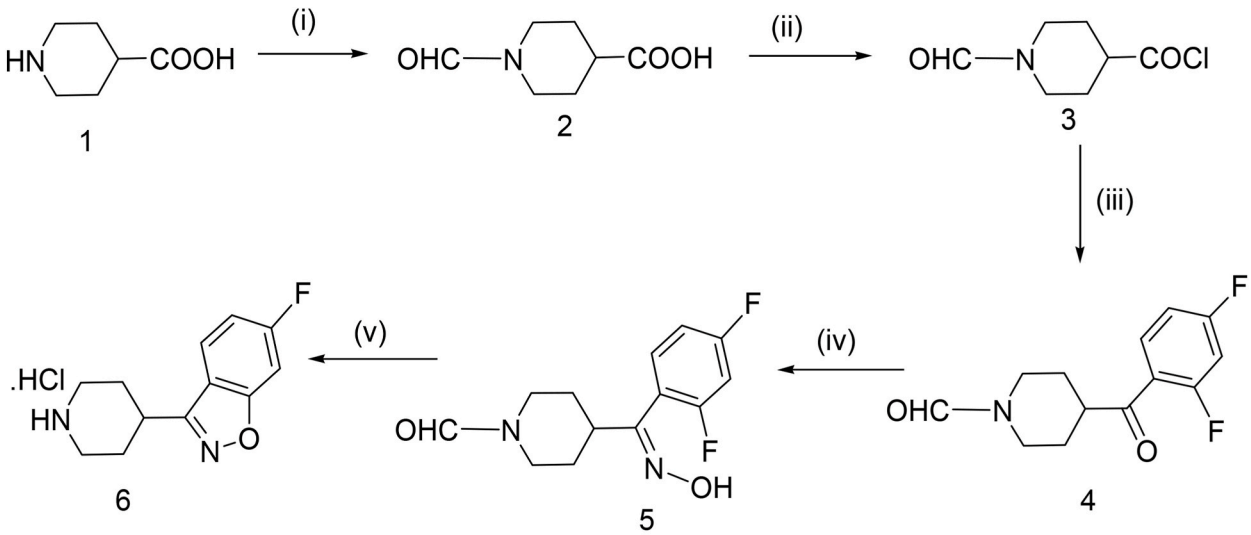

Scheme 1. Synthesis of FPBH **6**.

2.2. Synthesis of inhibitor

The compound FPBH **6** was prepared by literature procedure [17], as shown in Scheme 1.

Isonipecotic acid was formylated using formic acid/acetic anhydride mixture to give *N*-formyl isonipecotic acid **2**, which was heated with thionyl chloride to give acid chloride 3. The reaction of acid chloride **3** with 1,3-difluoro benzene in the presence of anhydrous $AlCl_3$ gave ketone **4**, which was converted to oxime **5** by oximation using hydroxylamine hydrochloride/sodium acetate. The formed oxime was refluxed with methanolic KOH followed by acidification with Aq. HCl results the title compound **6**: mp 302–304 °C; IR (KBr): 2144, 1612, 1460, 869 cm $^{-1}$; ^{1}H NMR (400 MHz, D_20): δ 2.0–2.2 (m, 4H, 2 X–CH2), 2.19 (d, 2H, -CH2), 2.83 (t, 2H, -CH2), 3.24–3.27 (m, 2H, –CH and –NH), 7.01 (d, 1H, Ar–H), 7.26 (t, 1H, Ar–H), 7.7 (d, 1H, Ar–H); ^{13}C NMR (D_20, 100 MHz): δ 29.6, 33.1, 33.4, 47.6, 48.1, 119.4, 122.2, 131.0, 132.1, 165.2, 166.2, 168.3.

2.3. Electrochemical techniques

The corrosion rate measurement was carried out by two extensively followed methods namely, EIS and PDP, and was achieved by means of a Potentiostat device (CH Instrument USA 604D) armed with the three-electrode system. Calomel, platinum, and MS coupons were taken as the reference, auxiliary, and working electrode respectively. The EIS parameters were determined by disrupting the steady state open circuit potential (OCP) with an amplitude of 10 mV ac signal (100 KHz–10 MHz) in order to generate Nyquist plots. The Tafel graphs are done by polarizing the specimen between −250 to +250 mV w.r.t OCP, maintaining a scan rate of 1 mV/s.

2.4. UV–Vis spectroscopic studies

The UV–visible spectrum of test solution having 5×10^{-5} M FPBH and solution in which MS specimen was immersed for 3 h were analyzed (1800 Shimadzu UV–Visible spectrophotometer).

2.5. FTIR spectroscopic studies

The IR spectrum of pure FPBH and the degraded product of the adsorbed FPBH coating on the MS surface are compared using FTIR spectrophotometer((Shimadzu-IR spirit).

2.6. Microscopic analysis

Using SEM (JEOL JSM-6380L) and AFM (1B342 Innova model), the microscopic studies of finely polished MS dipped in 0.5 M HCl containing FPHB were performed.

2.7. Quantum calculations and DFT

The DFT studies were done using the B3LYP/6–311++G(d,p) theory level [18,19]. In the calculation, geometry optimization was performed followed by the harmonic frequency calculation to ensure the molecule is in the global minimum of the potential energy surface. The molecular orbitals and their energies were also a part of DFT along with the molecular electrostatic potential calculation. Water as a solvent using the SCRF model has been used in all DFT calculations. The UV–Vis spectrum of FPBH is obtained by calculating vertical excitation energy using the time-dependent B3LYP (TD-B3LYP) theory. All the DFT calculations were performed using Gaussian 09 (rev. D) program suite [20].

The following relations were used to determine various theoretical parameters (Eqs. (1)–(6)),

$$IP = -E_{HOMO} \tag{1}$$

$$EA = -E_{LUMO} \tag{2}$$

$$\chi = ½\ (IP + EA) \tag{3}$$

$$\eta = ½\ (IP\text{-}EA) \tag{4}$$

$$\sigma = \frac{1}{\eta} \tag{5}$$

$$\Delta N = \frac{\varnothing_{Fe} - \chi inh}{2\eta inh} \tag{6}$$

Where *IP*, *EA*, χ, η, σ, and ΔN represent ionization energy, electron affinity, electronegativity, chemical hardness, chemical softness, and a fraction of electrons transferred respectively [21,22]. The work function, φ = 4.82 eV for iron surface is regarded as an appropriate indicator of the electronegativity of iron [23].

3. Discussion on results

3.1. Characterization of inhibitor

The inhibitor used for the study FPBH **6** was prepared by literature procedure [17] as shown in Scheme 1. The IR spectrum showed a broad peak at 3224 cm^{-1} for –NH stretching, 2964 cm^{-1} for –CH stretching, 1614 cm^{-1} for –C═N stretching, 1542 cm^{-1} for –C═C stretching and 1119 cm^{-1} for –C-F stretching. ^{1}H NMR showed three aromatic protons, a doublet at δ 7.7 ppm, a triplet at 7.26, and a doublet 7.01, which indicate the presence of three aromatic protons of 6-fluoro-1,2-benzisoxazole ring. A multiplet at δ 3.24–3.27 ppm for two protons is due to –CH and –NH protons of the piperidine ring and all the aliphatic –CH_2 groups appeared in the expected region. ^{13}C NMR also showed all the peaks for carbon atoms present on the ring in the expected region, which confirms the structure of the product.

3.2. PDP study

Fig. 1 portrays the polarisation curves for MS corrosion at various concentrations of FPBH at 303 K. The obtained numerical constraints such as i_{corr}, *CR*, E_{corr}, and the Tafel slopes with varied concentrations of the FPBH depicted in Table 1.

The obtained i_{corr} values were taken to determine the percentage inhibition efficiency (*IE*) (Eqs. (7)–(9)) [2].

$$IE(\%) = \frac{i_{corr} - i_{corr}(inh)}{i_{corr}} \times 100 \tag{7}$$

$$\text{CR}\left(mmy^{-1}\right) = \frac{3270 \times EW \times i_{corr}}{d} \tag{8}$$

Where, 3270-conversion factor, M-material's atomic mass, d-density (7.85gcm^{-3}), and Z-number of electrons transported.

$$\%IE = \frac{R_{ct(inh)} - R_{ct}}{R_{ct(inh)}} \times 100 \tag{9}$$

R_{ct} and $R_{ct(\text{inh})}$ is the charge transfer resistance in the absence and presence of FPBH respectively.

The clear observations of parameters in Table 1 indicate that the added concentrations of FPBH drastically decrease the i_{corr} and *CR*. The addition of 1×10^{-3} M FPBH reduced the density of corrosion current from 5.895 to 0.290 mA cm^{-2} and CR from 68.52 to 3.37 mmpy. This may be due to the hindering effect triggered by the adsorbed FPBH from the HCl medium. The increase in % IE is more distinct with the rise in FPBH concentration and showed a maximum IE of 95 % at its optimum concentration. The parallel Tafel slopes suggest the influence of FPBH on the rate of corrosion but not on the inhibition mechanism [24]. As per the reported work if the experimental variation of the E_{corr} value with the inhibitor is more than ±85 mV compared to blank may be viewed as cathodic or anodic [25]. The established shift in the E_{corr} value by 2–15 mV, cathodically suggests the influence of FPBH in impeding both metal oxidation and hydrogen evolution [26].

3.3. EIS study

The Nyquist plots of FPBH are portrayed in Fig. 2 (a). The plot at a higher frequency (HF) illustrates a single capacitive loop. The

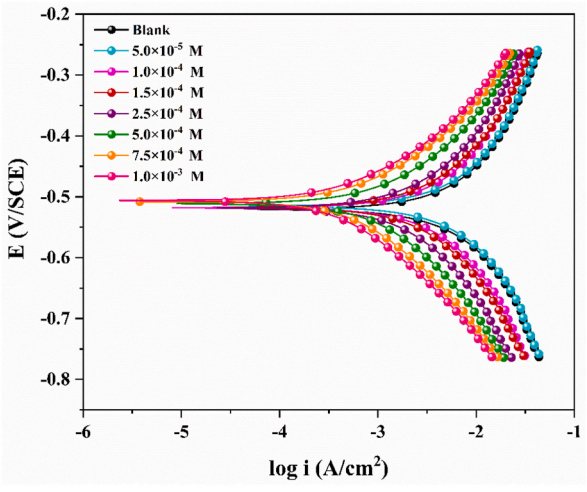

Fig. 1. Tafel plots for MS with and without FPBH at 303K.

Table 1
PDP data for MS corrosion with varied FPBH concentrations.

T (K)	FPBH Conc. M)	E_{corr} (V)	i_{corr} (mAcm$^{-2)}$	-β_c (mVdec^{-1})	$^{-}\beta_a$ (mVdec^{-1})	CR (mmpy)	IE (%)
303	Blank	−0.519	5.895 ± 0.020	55.5	5.065	68.52 ± 0.004	–
	5×10^{-5}	−0.515	3.658 ± 0.015	56.91	5.441	42.54 ± 0.003	37.9
	1×10^{-4}	−0.517	2.742 ± 0.021	59.06	6.447	31.87 ± 0.002	53.4
	1.5×10^{-4}	−0.515	1.915 ± 0.011	61.35	6.313	22.26 ± 0.001	67.5
	2.5×10^{-4}	−0.504	1.361 ± 0.032	70.83	8.191	15.82 ± 0.002	76.9
	5×10^{-4}	−0.511	0.969 ± 0.034	68.52	7.454	11.26 ± 0.003	83.5
	7.5×10^{-4}	−0.508	0.615 ± 0.015	68.07	8.000	7.15 ± 0.003	89.5
	1×10^{-3}	−0.504	0.290 ± 0.040	78.19	9.279	3.37 ± 0.001	95
313	Blank	−0.509	6.186 ± 0.010	54.34	5.099	71.93 ± 0.002	–
	5×10^{-5}	−0.513	4.175 ± 0.045	58.52	5.53	48.53 ± 0.001	32.5
	1×10^{-4}	−0.511	3.432 ± 0.051	58.85	5.676	39.9 ± 0.004	44.5
	1.5×10^{-4}	−0.503	2.483 ± 0.024	59.25	6.275	28.85 ± 0.005	59.8
	2.5×10^{-4}	−0.497	2.149 ± 0.061	60.96	6.379	24.99 ± 0.006	65.2
	5×10^{-4}	−0.503	1.877 ± 0.042	65.22	6.775	21.82 ± 0.004	69.6
	7.5×10^{-4}	−0.509	1.340 ± 0.028	67.73	6.95	15.58 ± 0.002	78.3
	1×10^{-3}	−0.527	1.069 ± 0.025	62.62	6.354	12.42 ± 0.004	82.7
323	Blank	−0.505	9.535 ± 0.021	51.77	5.002	110.87 ± 0.007	–
	5×10^{-5}	−0.503	7.224 ± 0.035	53.93	5.181	83.99 ± 0.003	24.2
	1×10^{-4}	−0.501	6.45 ± 0.025	55.24	5.234	74.98 ± 0.005	32.3
	1.5×10^{-4}	−0.508	5.324 ± 0.044	56.84	5.175	57.07 ± 0.002	44.1
	2.5×10^{-4}	−0.499	4.428 ± 0.52	58.00	5.751	51.48 ± 0.002	53.5
	5×10^{-4}	−0.507	3.54 ± 0.067	59.31	6.054	40.1 ± 0.005	62.8
	7.5×10^{-4}	−0.502	2.885 ± 0.024	61.18	6.251	33.55 ± 0.008	69.7
	1×10^{-3}	−0.500	2.695 ± 0.021	57.51	5.618	31.34 ± 0.003	71.7

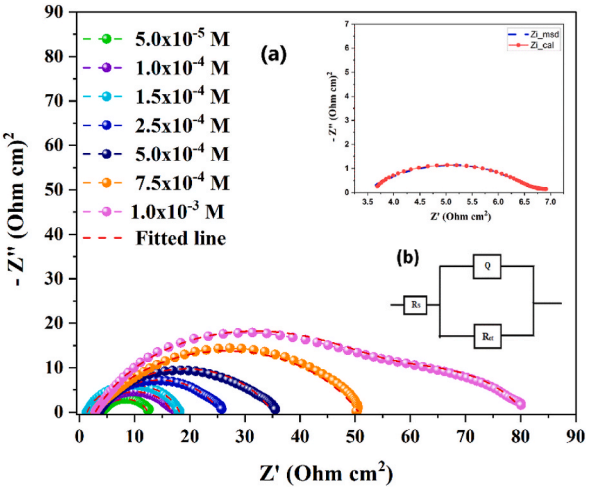

Fig. 2(a). Nyquist plots for MS with and without FPBH at 303K; Fig.2(b). An equivalent circuit was implemented to simulate the Nyquist plots.

one-time constant is exhibited by the equivalent Bode plot. From the single capacitive loop, it is seen that the oxidation of the metal surface in the corrosive medium studied is principally controlled by a charge transfer mechanism [27]. The difference between the higher and lower frequencies of the impedance yields the charge transfer resistance (R_{ct}). The solid electrodes corresponding to the capacitive loops are depressed owing to the surface roughness and buildup of the reaction product on the MS surface [28]. The lengthening of a semicircle in response to rising FPBH concentrations suggests an increase in the resistance towards the corrosion process [29].

Z-simpWin software was used to analyze EIS parameters by fitting the Nyquist plots to the relevant equivalent circuits, and the finest fit was observed with circuit RQR (with the $\chi^2 \leq 10^{-3}$) as represented in Fig. 2(b). It constitutes R_s as solution resistance, Q_1 as constant phase element (*CPE*). The rise in R_{ct} values in response to the rise in FPBH concentration was used to estimate inhibition efficiency *IE* (%) by Eq. (10) [30].

$$\%IE = \frac{R_{ct(inh)} - R_{ct}}{R_{ct(inh)}} \times 100 \tag{10}$$

The heterogeneity in the system made the use of *CPE* in place of double-layer capacitance (*Cdl*) to afford an exact match and the *CPE* of impedance is obtained by the given Eq. (11) [31].

$$z_{CPE} = Q^{-1}(iW_{max})^{-n} \tag{11}$$

Where, Q = proportionality coefficient, W_{max} = angular frequency, n = exponent related to phase shift ($0 \leq n \leq 1$), i signifies an imaginary number and n is equal to $\alpha/(\pi/2)$. If the n value is equal to 1, *CPE* is referred as the ideal capacitor. In the present case, the deviation of n values from unity is observed. This signifies the depressing nature of Nyquist plots because of the deposition of reaction products on the MS surface. Thus, by taking note of the frequency values at the highest imaginary component, the adjustment in the Cdl is determined and it is given by the relation (Eq. (12)) [32]. The resulting parameters are recorded in Table 2.

$$C_d = \frac{1}{2\pi R_{ct} f_{max}} \tag{12}$$

The decline in *Cdl* is observed due to the rise in the thickness of the Helmholtz double layer, which is created at the MS-solution interface [33]. This might be the result of the adsorption of FPBH on the metal electrode surface, by gradually replacing water molecules [34].

In the Bode plot (Fig. 3) the frequency values help in interpreting the nature of the electrochemical system. As it is shown in the Bode plot, the phase angle was increased with FPBH concentrations. This is attributed to the drop in metal dissolution owing to the demission in capacitive behavior of the MS surface. Also, the plot impedance |Z| against frequency exhibited two plateaus: one corresponds to a lower frequency and the other to a higher frequency. Low frequency is associated with R_{ct}, while high frequency is related to R_s [35]. In the Bode plot, the R_p values are computed from the difference between lower frequency (LF) and higher frequency (HF) and are observed to rise with FPBH concentrations [36].

3.4. Influence of temperature on corrosion rate

The CR values obtained from the PDP method at various temperatures are used to explore the activation and thermodynamic parameters. Arrhenius equation [37] is used to compute the energy of activation (E_a) (Eq. (13)) parameters.

$$ln(CR) = B - \frac{E_a}{RT} \tag{13}$$

R and B denote the gas constant and Arrhenius constant respectively. The graph of ln *CR* vs $1/T$ in Fig. 4(a) results in a straight line with a slope of $-E_a/R$, allowing the determination of Ea values. Using Eq. (14) [38], the enthalpy ($\Delta H^{\#}$) and entropy ($\Delta S^{\#}$) of activation were determined and reported in Table 3.

$$CR = \frac{RT}{Nh} exp\left(\frac{\Delta S^{\#}}{RT}\right) exp\left(\frac{-\Delta H^{\#}}{RT}\right) \tag{14}$$

h -Plank's constant and N-Avogadro's number.

A straight line is observed from a graph of ln (CR/T) vs $1/T$ (Fig. 4(b)).

Table 3 shows that adding FPBH successively increases Ea values due to physisorption. Moreover, the E_a value with and without the

Table 2
EIS data for the MS corrosion with varying FPBH concentrations.

T(K)	FPBH concentration(M)	R_S (Ω cm^2)	R_{ct}(Ω $cm^{2)}$	$\chi^2(10^{-3})$	C_{dl}(μFcm^{-2})	IE(%)
303	Blank	3.787	2.82 ± 0.35	1.04	49767.3	–
	5×10^{-5}	4.128	4.57 ± 0.23	0.57	11876.4	38.17
	1×10^{-4}	3.453	6.16 ± 0.24	1.22	5655.2	54.07
	1.5×10^{-4}	3.486	8.89 ± 0.45	1.41	2537.0	68.17
	2.5×10^{-4}	1.369	12.23 ± 0.42	4.48	2178.7	76.86
	5×10^{-4}	3.526	22.89 ± 0.52	1.24	733.96	85.71
	7.5×10^{-4}	2.748	31.25 ± 0.44	1.50	359.09	90.94
	1×10^{-3}	2.721	52.23 ± 0.61	4.60	172.92	94.58
313	Blank	3.194	2.09 ± 0.75	0.453	10453.3	–
	5×10^{-5}	3.301	3.18 ± 0.46	0.476	10044.6	34.28
	1×10^{-4}	3.230	4.01 ± 0.25	0.198	9255.0	47.97
	1.5×10^{-4}	3.022	5.33 ± 0.12	0.364	4341.0	60.82
	2.5×10^{-4}	3.822	6.52 ± 0.15	0.727	4251.3	67.94
	5×10^{-4}	3.247	7.89 ± 0.56	0.353	4166.1	73.50
	7.5×10^{-4}	3.792	11.26 ± 0.72	1.410	1941.7	81.42
	1×10^{-3}	2.767	14.46 ± 0.52	1.180	1263.4	85.53
323	Blank	3.166	1.35 ± 0.76	0.057	24257.4	–
	5×10^{-5}	3.075	1.76 ± 0.98	0.044	10782.3	23.12
	1×10^{-4}	3.227	2.11 ± 0.45	0.104	10470.1	35.79
	1.5×10^{-4}	2.975	2.53 ± 0.35	0.051	10262.8	46.48
	2.5×10^{-4}	3.067	3.13 ± 0.05	0.280	9018.62	56.74
	5×10^{-4}	2.986	4.02 ± 0.25	0.424	8783.44	66.31
	7.5×10^{-4}	3.066	5.13 ± 0.31	0.460	8592.37	73.59
	1×10^{-3}	4.072	5.58 ± 0.35	0.777	7902.88	75.71

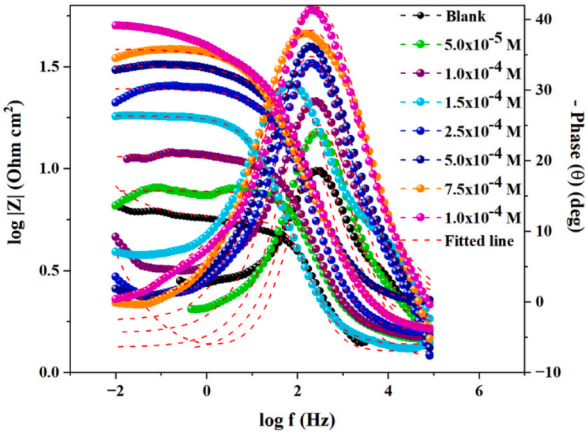

Fig. 3. Bode plots for MS with and without FPBH at 303K

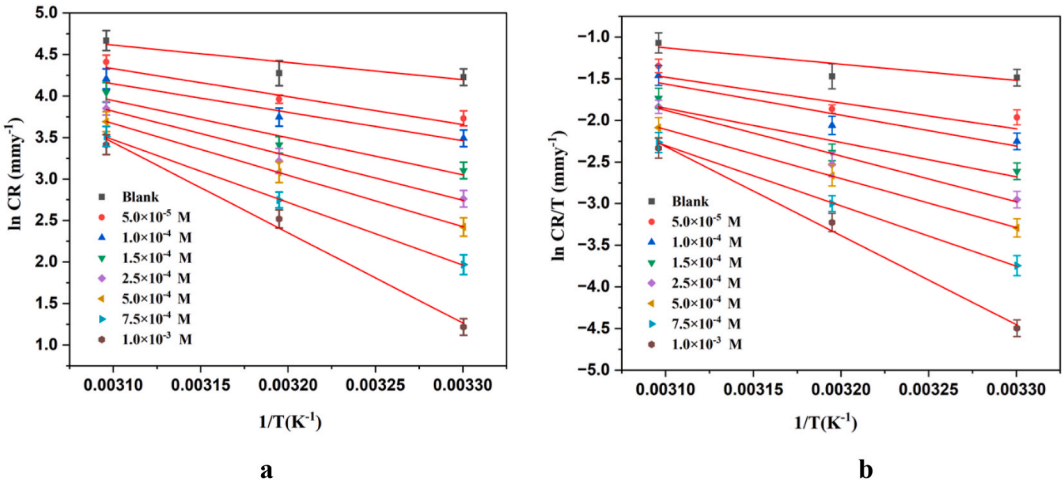

Fig. 4. (a) Plots of ln (*CR*) vs 1/*T* and **4(b)** Plot of ln (*CR/T*) vs 1/*T* at varying concentrations of FPBH.

Table 3
Activation parameter for MS corrosion at varying concentrations of FPBH.

FPBH concentration (M)	E_a(kJmol^{-1})	ΔH_a(kJmol^{-1})	ΔS_a(kJmol^{-1})
Blank	19.40	11.51	−171.68
5×10^{-5}	27.48	24.95	−131.86
1×10^{-4}	30.15	29.22	−120.21
1.5×10^{-4}	38.09	36.99	−97.59
2.5×10^{-4}	44.25	45.27	−73.06
5×10^{-4}	51.65	49.05	−62.97
7.5×10^{-4}	62.83	60.23	−29.91
1×10^{-3}	89.58	82.54	38.21

inhibitor FPBH is larger than 20 kJ/mol, signifying that the surface reaction controls the entire process. E_a values become more distinct with increasing FPBH concentration, demonstrating how the addition of an inhibitor reduces metal dissolution in acidic environment. According to this attribute, the protective layer that forms on the metal surface raises the energy barrier for corrosion to occur [39]. According to the obtained significant $\Delta S^{\#}$ values, the activated complex in the rate-determining phase signals an association rather than a dissociation [40].

3.5. Isotherm considerations

The adsorption behavior of FPBH at the MS-HCl interface is understood by choosing an appropriate isotherm. Several adsorption

isotherms are fitted using the degree of surface coverage (θ) data obtained from PDP experiments. The best association was found for Langmuir's isotherm and is given in Eq. (15) [41]. Kinetic-thermodynamic and Flory-Huggins models were also fitted into PDP results and the corresponding plots are given under Supplementary Fig. 1. Since the R^2 and slope values for these two isotherm models are deviating much from unity, indicating the adsorption of FPBH follows Langmuir's isotherm very well rather than Flory-Huggins models and kinetic-thermodynamic isotherm model. The obtained R^2 and slope values for all three isotherms are given under Supplementary Table 1..

$$\frac{C_{inh}}{\theta} = \frac{1}{K} + C_{inh} \tag{15}$$

Where, K_{ads} is the equilibrium constant and C is FPBH concentration.

The plot of $C_{(inh)}/\theta$ vs log C_{inh} (Fig. 5) displays a straight line. K values are calculated by using the intercept. The values of K are related to ΔG°_{ads}, represented by Eq. (16) [42] and reported in Table 4.

$$K = \frac{1}{55.5} exp\left(\frac{-\Delta G^{\circ}_{ads}}{RT}\right) \tag{16}$$

Where, R-Rydberg constant and 55.5 mol of water is present in the solution per cubic meter.

Using thermodynamic theory, the enthalpy (ΔH°_{ads}) and entropy (ΔS°_{ads}) of adsorption were computed (Eq. (17)) and reported in Table 4. Further, the obtained slope and linear association coefficient R^2 values are very close to unity suggesting an acceptable agreement between the obtained results and Langmuir's isotherm model.

$$\Delta G^{\circ}_{ads} = \Delta H^{\circ}_{ad} - T\Delta S^{\circ}_{ads} \tag{17}$$

The observed ΔG°_{ads} values lower than −20 kJ/mol suggest the adsorption of FPBH on the MS surface is owing to electrostatic interaction [42]. The -ve values of ΔH°_{ads} imply the mixed-type adsorption of FPBH molecules. The obtained ΔH°_{ads} are equal to −10.45 kJ/mol suggesting the interaction of FPBH is mainly through electrostatic interaction ie. Physisorption [43]. The FPBH molecules were randomly displaced in the solution prior to adsorption on the MS surface, as showed by the positive ΔS°_{ads} value, but as adsorption progressed, the FPBH equally adsorbed on the specimen surface, leading to a decrease in entropy [44].

3.6. UV–Vis spectroscopic study of FPBHs adsorption

As shown in Fig. 6, UV–Vis spectroscopy was utilized to examine the adsorption of FPBH on the MS surface. The UV–Vis spectrum of solution (5×10^{-5} M FPBH in 0.5 M HCl) was first recorded at RT, and it showed bands at 214, 248, and 312 nm owing to π→π* and n→π* transitions. After dipping the MS coupon for approximately 1 h, the UV–Vis spectra of the test solution of FPBH in 0.5 M HCl were performed. The lower absorption intensity in the spectrum shows that FPBH molecules have adhered to the metal surface.

4. Surface morphology studies

4.1. Scanning electron microscopic analysis

SEM studies were carried out to examine the accumulation of corrosion products. The polished MS coupons were made in contact with 0.5 M HCl for about 2 h without and with FPBH. The SEM images show the surface of a MS specimen of a freshly polished sample (Fig. 7 (a)) having a smooth and uniform surface, whereas acid immersed sample (Fig. 7 (b)) is heavily corroded and destroyed, with

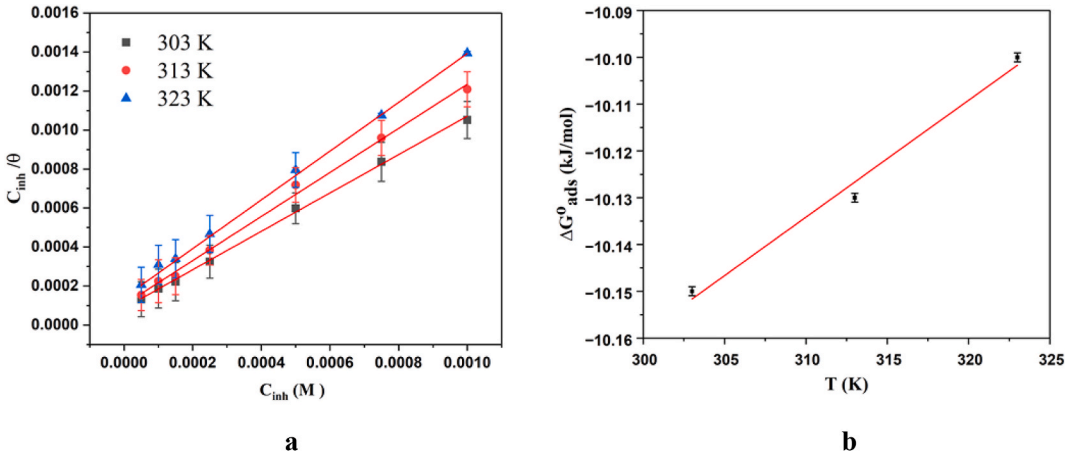

Fig. 5. (a) Plot of C_{inh}/θ vs C_{inh}, **5(b)** Plot of ΔG°_{ads} vs T (K) for MS in varying concentrations of FPBH.

Table 4
Thermodynamic factors for MS corrosion at various temperatures.

Temperature (K)	K_{ad}S (M^{-1})	Slope	R^2	ΔG°_{ads}(KJ mol^{-1})	ΔH^{o}_{ads}(KJ mol^{-1})	ΔS^{o}_{ads}(J $mol^{-1}K^{-1}$)
303	1.0161	0.9842	0.998	−10.15	−10.95	0.002
313	0.8859	1.1286	0.996	−10.13		
323	0.7762	1.2889	0.998	−10.10		

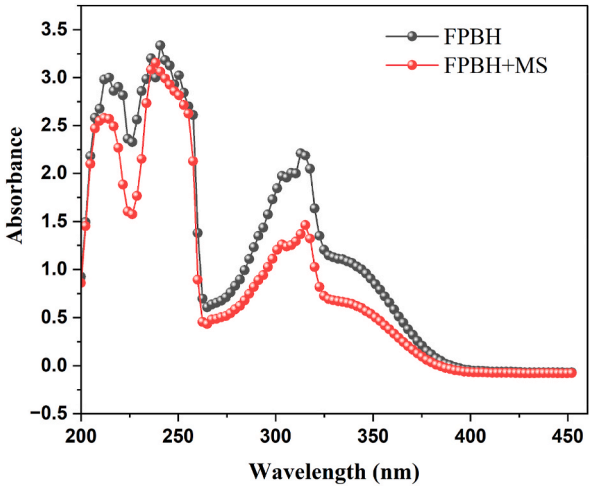

Fig. 6. UV–Visible absorption spectrum of a solution of 5×10^{-5} M FPBH in 0.5 M HCl without and with MS coupon.

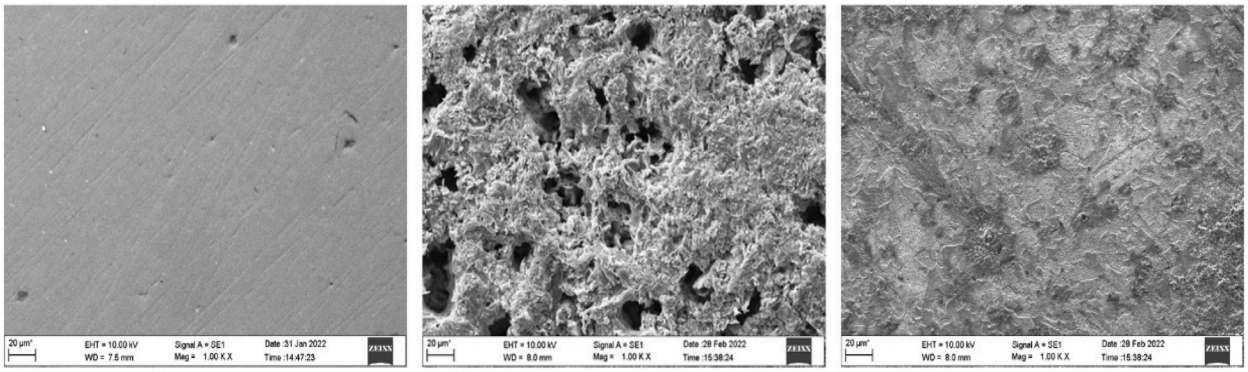

Fig. 7. (a) SEM image of freshly polished MS (b) SEM image of MS specimen dipped in 0.5 M HCl. (c) SEM image of MS specimen dipped in inhibitor solution (0.5 M HCl + FPBH).

horny spike-like features caused by acidic ions directly attacking the steel. The protected sample (Fig. 7 (c)) shows a smooth and uniform surface with less damage when compared to the unprotected sample. This shows the inhibitory potential of FPBH over the MS surface.

4.2. Atomic force microscopic analysis

For surface topography experiments, the MS specimen was submerged in acid medium containing FPBH for 2 h. The relevant AFM images are displayed in Fig. 8(a–c). For freshly polished surfaces, the average surface roughness (R_a) and root mean square roughness (R_q) values were 7.67 nm and 11.0 nm, respectively, but the R_a and R_q values for samples dipped in 0.5 M HCl were 182 nm and 236 nm, respectively. The average R_a and R_q values obtained for the sample immersed in inhibitor solution are 37.4 nm and 46.9 nm respectively. The results presented above make it clear that the inhibited sample's R_a and R_q values are lower than those of the un-inhibited sample. This describes how the FPBH adhered to the specimen surface.

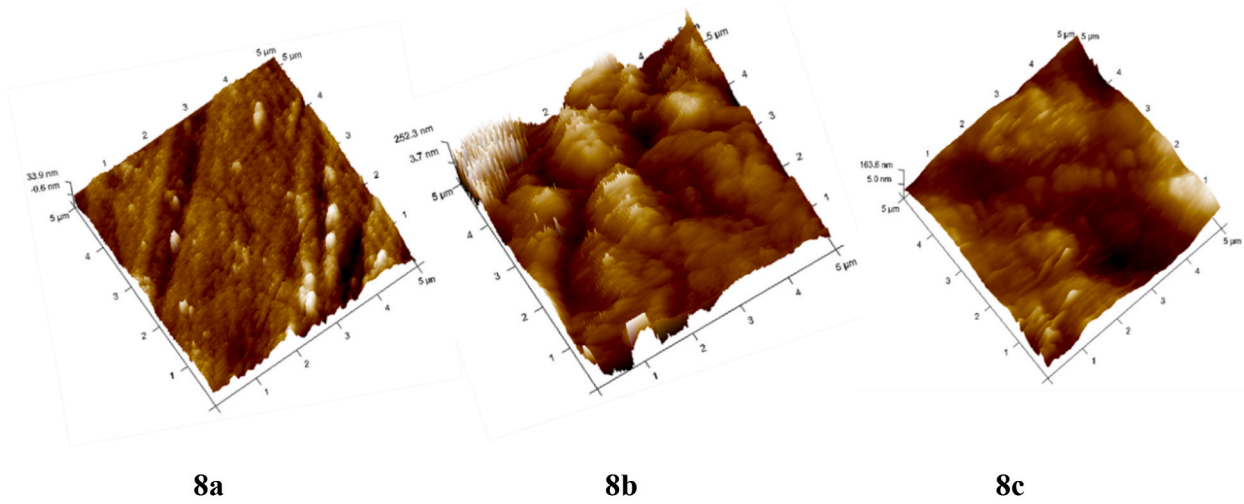

Fig. 8. (a) AFM image of freshly polished MS (b) AFM image of MS specimen dipped in 0.5 M HCl (c) AFM image of MS in 0.5 M HCl + FPBH inhibitor.

5. Density functional theory (DFT)

5.1. Geometry optimization and FMO theory

DFT calculations were made to comprehend the factors affecting the efficiency of an inhibitor. Fig. 9 shows the optimized geometry of the molecule obtained using the B3LYP/6–311++G(d,p) method. In the optimized structure, the piperidine ring shows chair conformation which is energetically more stable compared to the boat conformation. The frontier molecular orbitals of the molecule, HOMO and LUMO are shown in Fig. 10. As it is evident, the HOMO is mainly from the lone pair on the N-atom in the piperidine ring whereas in LUMO electron density is of π* characteristic and located on benzisoxazole part of the molecule [18,19]. The quantum chemical calculations deliver more evidence regarding the structural features of FPBH, whereas the reactivity of the compound is taken into account by the adsorption mechanism.

In the study, geometrical optimization and FMO theory are convenient in predicting the nature and amount of FPBH adsorption on the surface [45]. The quantum chemical factors calculated such as E_{HOMO}, E_{LUMO}, the energy gap (ΔE_{gap}), and the number of electrons transferred (ΔN) are significant and valuable factors to relate the corrosion inhibitory ability of FPBH. These quantum chemical parameters are also very useful to authenticate the results obtained experimentally. The theoretical results obtained are shown in Table 5. The HOMO and LUMO are shows the good electron-donating ability of FPBH molecules to the suitable acceptor and also show its power to receive electrons from metals. The E_{LUMO} is a measurement of a molecule's propensity to accept an electron from the donor species, whereas the E_{HOMO} is a measure of a molecule's capacity to transfer an electron to an acceptor [46]. Better electron donation propensity of the inhibitor is indicated by a higher value of E_{HOMO} and better tendency of a molecule to accept electrons is specified by lower E_{LUMO} values [47]. The ΔE_{gap} is also a significant factor in recognizing the chemical reactivity of an inhibitor and its ability to be an active corrosion inhibitor [48]. Since removing an electron from the final occupied orbital requires less energy, the effectiveness of the adsorption between the inhibitors and metal surface rises as ΔE_{gap} lowers [49]. It is observed from Table 5, that the higher energy gap value for FPBH ($\Delta E_{gap} = 4.72$) indicates the greater adsorption performance of FPBH. Similarly, E_{LUMO} values signify the capability of the inhibitor to receive electrons. The value of ΔN specifies the capacity of the studied inhibitor to donate its electrons to the metal when $\Delta N > 0$ and vice versa when $\Delta N < 0$. As per this convention, it is clear from Table 5, that FPBH has a higher propensity to contribute electrons to the metallic surfaces [50,51].

Another important factor that helps to understand why atoms and molecules are chemically reactive is their ionization potential. The easier it is to remove an electron from a molecule, the lower its ionization potential value is, while a greater ionization potential value specifies that the molecule is highly stable and chemically inert [52]. Based on acid-base theory, the explanation of the hard and soft acid/base is related to the chemical softness and hardness properties. A soft molecule is likely to have the highest level of inhibitory efficiency since soft molecules have the highest tendency to respond while hard molecules have the lowest tendency to do so [53].

The induced dipole moment to electric field intensity ratio is known as polarizability. Polarizability and the induced dipole moment are inversely related. The corrosion inhibition direction is also assessed using the dipole moment. The distribution of electrons within a molecule is related to the dipole moment, which gives the polarity in a bond [54]. There is a general consensus that polar molecules with strong dipole moments adsorbed on the MS surface can increase the effectiveness of inhibitory action. However, the literature is inconsistent in predicting corrosion inhibition direction using dipole moment.

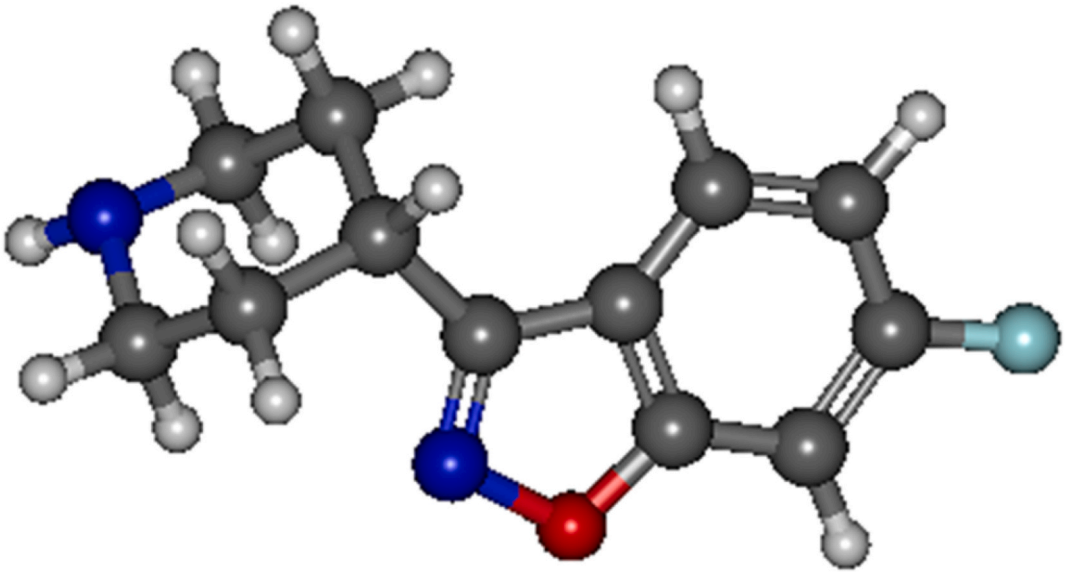

Fig. 9. Optimized structure of FPBH using B3LYP/6–311++G(d,p) method.

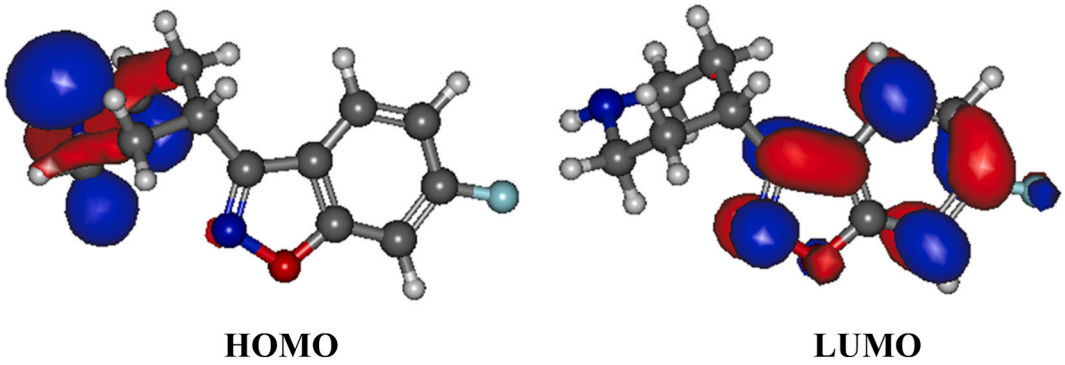

Fig. 10. FMO (HOMO and LUMO) of inhibitor FPBH.

Table 5
B3LYP/6–311++G(d,p) calculated parameter values for inhibitor FPBH.

Parameters	Parameter values
HOMO (eV)	−6.358
LUMO (eV)	−1.638
Energy Gap (ΔE_{gap}) (eV)	4.72
Ionization potential (*IP*) (eV)	6.358
Electron Affinity (*EA*)(eV)	1.638
Electronegativity (χ) (eV)	3.998
Chemical Potential (μ) (eV)	−3.998
Chemical Hardness(η) (eV)	2.36
Chemical Softness ($1/\eta$) (eV)	0.424
Electrophilicity ($\omega = \mu^2/\eta$) (eV)	6.773
Polarizability (α) (a.u)	206.70
Dipole moment (Debye)	3.219

5.2. Molecular electrostatic potential (MEP)

The MEP is a reliable diagnostic tool for hydrogen bond, electrophile, and nucleophile interaction sites. MEP modeling was considered a highly helpful tool for the investigation of the association between the structure of a compound and its physico-chemical properties or interactions with the metal surface [55]. Fig. 11 shows the MEP profile of the inhibitor used in this study. Several colors

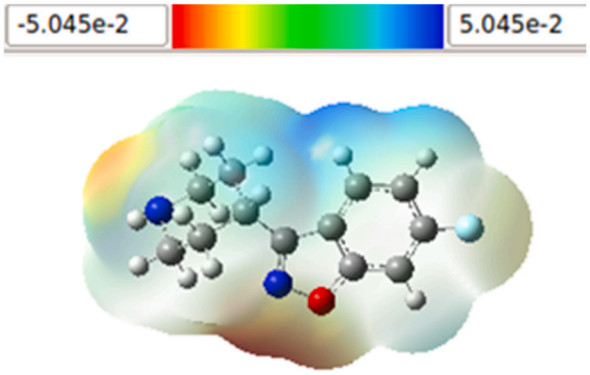

Fig. 11. MEP surface map calculated for the title compound.

were used to examine the MEP map; red-denoted areas with the least, blue regions with the maximum, and green regions with zero electrostatic potential respectively. MEP graphic reveals how the potential varies as the colors move from blue ⟶ green⟶ yellow⟶ orange⟶ red⟶ blue [56]. Electrostatic potential regions that are related to electrophilic and nucleophilic behavior are shown in red and blue, respectively. The MEP image of FPBH has a color coding zone that ranges from $-5.045e^{-2}$ to $5.045e^{-2}$. The presence of an effective nitrogen location is considered one possible site for nucleophilic attack. From Fig. 13, it is clear that the C–O has the highest electrostatic potential, which is denoted by the deep red color. This suggests a severe lack of electrons and, hence, a prospective location for the electrophilic region.

5.3. UV analysis

The UV–Vis electronic spectrum of FPBH is also calculated theoretically using time-dependent (TD-B3LYP/6–311++G(d,p)) theory [57]. For the calculation, vertical excitation was used from the ground state optimized geometry, and ten low-energy singlet excited states were computed. Fig. 12 shows the calculated UV–Vis spectrum of FPBH, and Table 6 lists the parameters of the five lowest singlet excited states. The first excited state represents the HOMO→LUMO transition and has a very small oscillator strength due to the optically forbidden n→π* transition. The calculated band gap was 4.15 eV. The optically allowed transitions are $S_0 \rightarrow S_2$ with key contribution from HOMO-2→LUMO, $S_0 \rightarrow S_3$ from HOMO-1→LUMO and $S_0 \rightarrow S_4$, from HOMO→LUMO+1. Corresponding transition wavelengths for these three transitions are 255, 240 and 235 nm, respectively. Corresponding absorption bands can also be seen in the spectrum shown in Fig. 12. Overall this study indicated that the title compound undergoes electron stimulation and energy transfer [58].

The title molecule's UV–Vis electronic spectrum is obtained theoretically (TD-B3LYP/basis set) [57]. Lambda (λ) max values of the title compound are 311 are revealed via theoretical UV–Vis spectral data, and its band gap is 4.032. Table 6 lists the analyzed structure's oscillation strength, band gap energy, and excitation energy. Fig. 12 shows the UV computed spectrum. The HOMO-LUMO band gap and the bandgap computed from the electronic spectrum have good correlations. This study indicated that the title compound undergoes electron stimulation and energy transfer. The important transitions π⟶π*, n⟶ π*, and n⟶π* will change in direction towards a higher wavelength in the first case and towards a shorter wavelength in the final two cases as the solvent polarity increases [58].

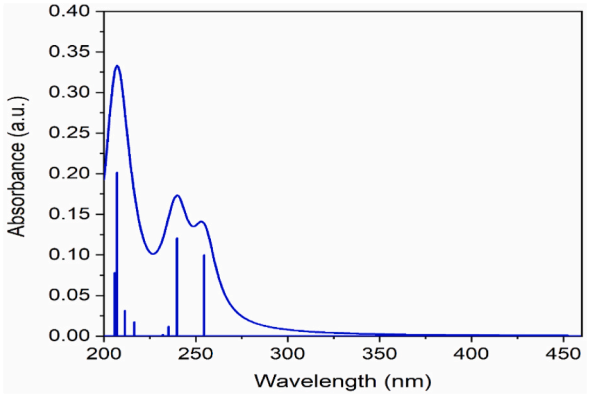

Fig. 12. TD-B3LYP/6–311++G(d,p) calculated UV–Vis spectrum of FPBH.

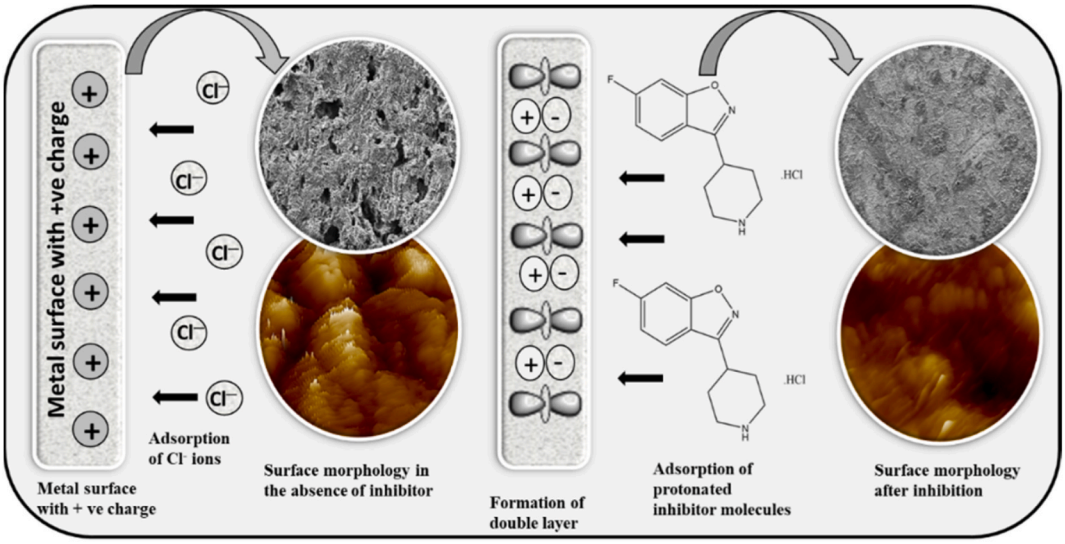

Fig. 13. Physical adsorption of FPBH molecules on the MS surface.

Table 6
TD-B3LYP/6–311++G(d,p) calculated UV–Vis constraints of FPBH.

Excited states	Transition wavelength (λmax) (nm)	Band Gap (eV)	Oscillator strength	Assignment (Co-efficient)
$S_0 \longrightarrow S_1$	299	4.1509	0.0002	HOMO ⟶ LUMO (0.705)
$S_0 \longrightarrow S_2$	255	4.8709	0.0998	HOMO-2⟶LUMO (0.614)
				HOMO-1⟶LUMO (0.194)
				HOMO-1⟶LUMO+1 (0.265)
$S_0 \longrightarrow S_3$	240	5.1705	0.1206	HOMO-2⟶LUMO (0.158)
				HOMO-2⟶LUMO+1 (0.161)
				HOMO-1⟶LUMO (0.629)
				HOMO⟶LUMO+1 (0.173)
$S_0 \longrightarrow S_4$	235	5.2706	0.0117	HOMO-1⟶LUMO (0.147)
				HOMO⟶LUMO+1 (0.681)
$S_0 \longrightarrow S_5$	232	5.3415	0.0020	HOMO⟶LUMO+2 (0.623)
				HOMO⟶LUMO+3 (0.184)
				HOMO⟶LUMO+4 (0.242)

5.4. Comparison of inhibition efficiency of the investigated compound with reported azole derivates

Table 7 shows the performance inhibition efficiency of the FPBH molecule in comparison with some of the reported azole derivatives including oxazoles. Since FPBH exhibits essentially identical inhibitory efficacies to those of other known inhibitors of this class, it has been demonstrated to be a viable inhibitor for halting MS corrosion.

5.5. Corrosion inhibition mechanism

A single mechanism is not able to elucidate the corrosion inhibition method. The experimental conditions could alter the mechanism. The interaction of added FPBH on the MS surface can take place via one or more of the succeeding modes. (1) The interaction among the positively charged metal surface and protonated inhibitor, (2) The electron lone pairs on inhibitor with empty d- orbitals of Fe atoms, (3) π-electrons of aromatic ring with the empty d-orbitals of Fe atoms [2]. In this case, the adsorption of FPBH molecules principally takes place through a physical mode of adsorption, as explained by the adsorption isotherms.

In the current study, (i) the working specimen in contact with acid medium gets + ve charge due to initial oxidation. (ii) The Cl^- ions are then attracted towards the +vely charged specimen surface and result in the creation of a double layer (Helmholtz electric layer) at the metal electrode-acid interface. (iii) The added FPBH molecules get protonated in acid medium and are attracted toward the negative charge of the double layer via electrostatic interaction [70]. The graphical representation of the electrostatic interactions is revealed in Fig. 13.

6. Conclusion

The outcomes of the several methods presented here support the potential of FPBH as a viable water-soluble inhibitor for the acid

Table 7
Evaluation of the reported azole compounds as corrosion inhibitors in comparison to FPBH.

Acid media	Sample	Inhibitor	Temp.	% IE at optimum concentration	Method. Adsorption isotherm and type of inhibitor	Ref
1 M HCl	Mild steel	IOD	303 K	96.7 % at 300 ppm	PDP and EIS Langmuir adsorption isotherm, Mixed type	[59]
0.1 M H_2SO_4	Mild steel	BI ABI PBI OP)	303 K	BI = 38 % ABI = 6.38 % PBI = 85.23 % OP = 98.64 % at 0.001 M	PDP and EIS IE is in the order of OP > PBI > ABI > BI	[60]
2 M HCl	Mild steel	P PI	303 K	P = 66 PI = 80 at 0.001 M	PDP and EIS Temkin adsorption isotherm	[61]
1 M HCl	Mild steel	OC1 OC2 OC3	303 K	OC1 = 78.6 % OC2 = 94.7 % OC3 = 85.9 % at 0.001 M	PDP and EIS Langmuir's adsorption Mixed type	[62]
1 M HCl	Mild steel	PBO BOQ FMPBO	303 K	PBO = 88 % BOQ = 94 % FMPBO = 92 % at 0.002 M %IE in the order of L2 >L3 >L1.	PDP and EIS Langmuir's adsorption	[63]
1 M H_2SO_4	Mild steel	PPP POP	303 K	PPP = 91.99 % POP = 91.6 % at 1 mM	Weight loss DFT	[64]
1 M HCl	Carbon steel	BTH BTAH BI	303 K	BTH = 88.4 % BTAH = 82.7 % BI = 8 %	PDP and EIS Langmuir's adsorption Mixed type	[65]
1 M HCl	Mild steel	PAP APP	303 K	PAP = 86 % APP = 85 % at 0.001 M	PDP and EIS Langmuir's adsorption Mixed type	[66]
1 M HCl	C38 steel	BT39 BT40 BT45	303 K	BT39 = 56 % BT40 = 62 % BT45 = 86 % At 0.001 M	PDP and EIS Langmuir adsorption	[67]
0.5 M HCl	Mild steel	BPOX	303 K	BPOX = 95 % at 0.005 M	PDP and EIS and weight loss Langmuir adsorption Physisorption	[33]
1 M HCl	Mild steel	2B54NPO 24MO5POO	298 K	2B54NPO = 94.08 % 24MO5POO = 92.37 % for at 300 ppm	PDP and EIS and weight loss Langmuir adsorption	[68]
1 M HCl	N18 steel	BOP BOPO QBO	303 K	BOP = 59.4 % BOPO = 82.4 % QBO = 85.21 At 0.001 M	PDP, EIS and DFT	[69]
0.5 M HCl	Mild steel	FPBH	303 K	FPBH = 95 % at 0.001 M	PDP and EIS and DFT Langmuir adsorption	Prsent study

corrosion of MS. According to the PDP investigations, the icorr as well as CR significantly decreased after introducing FPBH to the test solution and showed IE of 95 % at $1 \times 10-3$ M FPBH. Furthermore, by adhering to Langmuir's adsorption isotherm, the compound FPBH can be termed as a mixed-type inhibitor. According to EIS tests, adding FPBH to a corrosive solution results in a significant rise in polarisation resistance and a concurrent decrease in the Cdl values. The physisorption of FPBH on the MS surface is supported by thermodynamic characteristics. An improved picture of the evaluated inhibitors' reactivity towards mild steel is provided by FMO experiments. In a parallel adsorption arrangement, it has been observed that FPBH adsorbed on the iron surface using heteroatoms (*N* and *O*) and π-electrons. The MEP modeling has shown how the inhibitor's molecular structure relates to its physico-chemical properties and interactions with the MS surface.

CRediT authorship contribution statement

Preethi Kumari P: Conceptualization, Data curation, Writing – original draft. **Anusha G:** Data curation, Investigation, Methodology. **J.N Cheerlin Mishma:** Data curation, Software. **Rajeev K. Sinha:** Formal analysis, Software, Validation. **Aishwarya S. Suvarna:** Data curation, Methodology. **Santosh L. Gaonkar:** Conceptualization, Project administration, Resources, Supervision, Writing – review & editing.

Declaration of competing interest

The authors declare that they have no known competing financial interests or personal relationships that could have appeared to influence the work reported in this paper.

Appendix A. Supplementary data

Supplementary data to this article can be found online at https://doi.org/10.1016/j.heliyon.2023.e21014.

References

[1] Z. Tao, S. Zhang, W. Li, B. Hou, Corrosion inhibition of mild steel in acidic solution by some oxo-triazole derivatives, Corrosion Sci. 51 (11) (2009) 2588–2595.
[2] V.C. Anadebe, V.I. Chukwuike, V. Selvaraj, A. Pandikumar, R.C. Barik, Sulfur-doped graphitic carbon nitride (S-g-C3N4) as an efficient corrosion inhibitor for X65 pipeline steel in CO2- saturated 3.5% NaCl solution: electrochemical, XPS and Nanoindentation Studies, Process Saf. Environ. 164 (2022) 715–728.
[3] V. C Anadebe, P.C. Nnaji, O. D Onukwuli, N.A. Okafor, F.E. Abeng, V.I. Chukwuike, C.C. Okoye, I.I. Udoh, M.A. Chidiebere, L. Guo, R.C. Bariky, Multidimensional insight into the corrosion inhibition of salbutamol drug molecule on mild steel in oilfield acidizing fluid: experimental and computer aided modeling approach, J. Mol. Liq. 349 (2022), 118482.
[4] P.P. Kumari, P. Shetty, S.A. Rao, Electrochemical measurements for the corrosion inhibition of mild steel in 1 M hydrochloric acid by using an aromatic hydrazide derivative, Arabian J. Chem. 10 (2017) 653–663.
[5] P.P. Kumari, P. Shetty, S.A. Rao, D. Sunil, T. Vishwanath, Synthesis, characterization and anticorrosion behaviour of a novel hydrazide derivatives on mild steel in hydrochloric acid medium, Bull. Mater. Sci. 43 (2020) 46.
[6] P.P. Kumari, P. Shetty, S.A. Rao, Corrosion inhibition effect of 4-Hydroxy-N'-[(E)-(1H-indole-2-ylmethylidene)] benzohydrazide on mild steel in hydrochloric acid solution, Int. J. of Corros. (2014) 11. Article ID 256424.
[7] M.Y. El Sayed, A.M. Abdel-Gaber, R.T. Rahal, Safranin—a potential corrosion inhibitor for mild steel in acidic media: a combined experimental and theoretical approach, J. Fail. Anal. Prev. 19 (2019) 1174–1180.
[8] R.T. Rahal, A.M. Abdel-Gaber, G.O. Younes, Inhibition of steel corrosion in nitric acid by sulfur-containing compounds, Chem. Eng. Commun. 203 (4) (2016) 435–445.
[9] P.P. Kumari, P. Shetty, S.A. Rao, D. Sunil, Inhibition behaviour of 2-[(2-methylquinolin-8-yl) oxy] acetohydrazide on the corrosion of mild steel in hydrochloric acid solution, Trans. Indian Inst. Met. 70 (4) (2017) 1139–1150.
[10] M.A. Hegazy, H.M. Ahmed, A.S. El-Tabei, Investigation of the inhibitive effect of p-substituted 4-(N, N, N-dimethyl dodecyl ammonium bromide)benzylidene-benzene-2-yl-amine on corrosion of carbon steel pipelines in acidic medium, Corrosion Sci. 53 (2011) 671–678.
[11] K.P. Rakesh, C.S. Shantharam, M.B. Sridhara, H.M. Manukumar, Hua-Li Qin, Benzisoxazole: a privileged scaffold for medicinal chemistry, Med.chem.comm. 8 (11) (2017) 2023–2039.
[12] Y.G. Gelders, S.L.E. Heylen, B.G. Vander, A.J.M. Reyntjens, P.A. Janssen, Pilot clinical investigation of risperidone in the treatment of psychotic patients, J. Pharmacopsychiatry. 23 (1990) 206–211.
[13] Y. Uto, 1,2-Benzisoxazole: a privileged structure with a potential for Polypharmacology, Curr. Pharm. Des. 22 (21) (2016) 3201–3211.
[14] K.E. Essien, A.O. Odiongenyi, E.J. BoEkom, E.J. Abai, et al., Corrosion inhibition potential of two isoxazole derivatives: experimental and theoretical Analyses, J. Mater. Environ. Sci. 13 (8) (2022) 928–944.
[15] A. Kumar, S. Nanjundaswamy, S.L. Gaonkar, B.P. Salimath, K.S. Rangappa, N-substituted-2-butyl-5-chloro-3H-imidazole-4-carbaldehyde derivatives as anti-tumor agents against Ehrlich ascites tumor cells in vivo, Med. Chem. 3 (3) (2007) 269–276.
[16] S. L, K.M. Gaonkar, L. Rai, A new method for the generation of azoalkenes from ketohydrazones and its application to the synthesis of tetrahydropyridazine derivatives, Tetrahedron Lett. 46 (35) (2005) 5969–5970.
[17] S.B.B. Prasad, K. Vinaya, C.S.A. Kumar, S. Swarup, K.S. Rangappa, Synthesis of novel 6-fluoro-3-(4-piperidinyl)-1,2-benzisoxazole derivatives as antiproliferative agents: a structure-activity relationship study, Invest New Drugs 27 (6) (2009) 534–542.
[18] G.A. Petersson, A. Bennett, T.G. Tensfeldt, et al., A complete basis set model chemistry; I. The total energies of closed-shell atoms and hydrides of the first-row elements, J. Chem. Phys. 89 (1988) 2193–2218.
[19] C. Lee, W. Yang, R.G. Parr, Development of the Colle-Salvetti correlation-energy formula into a functional of the electron density, Phys. Rev. B 37 (2) (1988) 785–789.
[20] M.J. Frisch, G.W. Trucks, H.B. Schlegel, G.E. Scuseria, M.A. Robb, et al., Gaussian 09, Revision D.01, Gaussian, Inc., Wallingford CT, 2013.
[21] B. Gomez, N. Likhanova, M. Dominguez-Aguilar, et al., Quantum chemical study of the inhibitive properties of 2-pyridyl-azoles, J. Phys. Chem. B 110 (2006) 8928–8934.
[22] Z. Cao, Y. Tang, F. Zhang, et al., Novel benzimidazole derivatives as corrosion inhibitors of mild steel in the acidic media. Part II: theoretical studies, Corrosion Sci. 83 (2014) 292–298.
[23] Y. Bhatt, P.P. Kumari, D. Sunil, S.A. Rao, P. Shetty, S. Kagatikar, The impact of naphthalimide derivative on the mitigation of mild steel corrosion in sulfamic acid medium: experimental and theoretical insights, Chem. Pap. 75 (2021) 3831–3845.
[24] R.K. Gupta, M. Malviya, K.R. Ansari, H. Lgaz, D.S. Chauhan, M.A. Quraishi, Functionalized Graphene oxide as a new generation corrosion inhibitor for industrial pickling process: DFT and experimental approach, Mater. Chem. Phys. 236 (2019), 121727.
[25] D. Sunil, P.P. Kumari, P. Shetty, S. A Rao, Indole hydrazide derivatives as potential corrosion inhibitors for mild steel in HCl acid medium: experimental study and theoretical calculations, Trans. Indian Inst. Met. 75 (1) (2022) 11–25.
[26] L.W. El Khatib, H.T. Rahal, A.M. Abdel-Gaber, Synergistic effect between Fragaria ananassa and Cucurbita pepo L Leaf Extracts on mild steel corrosion in hydrochloric acid solutions, Prot. Met. Phys. Chem. 56 (5) (2020) 1096–1106.
[27] Y. Elouadi, A. Bouyanzer, R. Touzani, F. Abrigach, Corrosion inhibition of mild steel by new N-heterocyclic compound in 1 M HCl: experimental and computational study, Der Pharma Chem. 7 (8) (2015) 265–275.
[28] P.S. Desai, N.S. Indorwala, Triazoles used as a Corrosion inhibitor for mild steel in Hydrochloric Acid, Int. J. Curr. Microbiol. Appl. Sci. 4 (2) (2015) 929–938.
[29] S.B. Benaka Prasad, K. Vinaya, C.S. Ananda Kumar, S. Swarup, K.S. Rangappa, Synthesis of novel 6-fluoro-3-(4-piperidinyl)-1,2-benzisoxazole derivatives as antiproliferative agents: a structure-activity relationship study, Invest. New. Drugs. 27 (6) (2009) 534–542.
[30] C. Verma, M.A. Quraishi, L.O. Olasunkanmi, E. Ebenso, L-Proline-promoted synthesis of 2-amino-4-Arylquinoline-3-Carbonitriles as sustainable corrosion inhibitors for mild steel in 1 M HCl: experimental and computational studies, RSC Adv. 5 (104) (2015) 85417–85430.
[31] Y. Elouadi, A. Bouyanzer, R. Touzani, F. Abrigach, Corrosion inhibition of mild steel by new N-heterocyclic compound in 1 M HCl: experimental and computational study, Der Pharma Chem. 7 (8) (2015) 265–275.
[32] M. Bairy, M. Pais, P.P. Kumari, S.A. Rao, Hydrazine carbothioamide derivative as an effective inhibitor for corrosion control: electrochemical, surface and theoretical studies, Journal of Bio- and Tribo-Corrosion. 8 (5) (2022).
[33] G. Moretti, F. Guidi, F. Fabris, Corrosion inhibition of the mild steel in 0.5 M HCl by 2-Butyl-Hexahydropyrrolo[1,2-b][1,2]Oxazole, Corros, Sci 76 (2013) 206–218.
[34] H. Rahmani, K.I. Alaoui, K.M. Emran, A. Hallaoui, et al., Experimental and DFT investigation on the corrosion inhibition of mild steel by 1,2,3-triazolereg iosomers in 1M hydrochloric acid solution, Preprints.org. 2018030116 (2018), https://doi.org/10.20944/preprints201803.0116.v1.
[35] L. Guo, S.T. Zhang, T.M. Lv, W.J. Feng, Comparative theoretical study on the corrosion inhibition properties of benzoxazole and benzothiazole, Res. Chem. Intermed. 41 (6) (2015) 3729–3742.
[36] K. Kalaiselvi, N. Saranya, B.A. Mallika, J. Piperidine and bispiperidine as corrosion inhibitor on mild steel in 1N hydrochloric acid medium, Int. J. Eng. Res. 5 (6) (2014) 275–286.

[37] A.A. Alamiery, Study of corrosion behavior of N'-(2-(2-Oxomethylpyrrol-1-Yl)Ethyl)piperidine for mild steel in the acid environment 12 (3) (2022) 3638–3646.
[38] J. Aslam, R. Aslam, S.H. Alrefaee, M. Mobin, A. Aslam, M. Parveen, C. Mustansar Hussain, Gravimetric, electrochemical, and morphological studies of an isoxazole derivative as corrosion inhibitor for mild steel in 1M HCl, Arabian J. Chem. 13 (11) (2020) 7744–7758.
[39] M. Jeeva, G. Venkatesa Prabhu, C.M. Rajesh, Inhibition effect of nicotinamide and its mannich base derivatives on mild steel corrosion in HCl, J. Mater. Sci. 52 (21) (2017) 12861–12888.
[40] H. Rahmani, F. El-Hajjaji, A. Hallaoui, M. Taleb, Z. Rais, M. Azzouzi, B. Labriti, K.I. Alaoui, B. Hammouti, Experimental, quantum chemical studies of oxazole derivatives as corrosion inhibitors on mild steel in molar hydrochloric acid medium, Int. J. Corros. Scale Inhib. 7 (4) (2018) 509–527.
[41] N.G. Poojary, P. P Kumari, S.A. Rao, 4-Hydroxyl-N0-[(3-Hydroxy-4-Methoxyphenyl) Methylidene] Benzohydrazide] as Corrosion inhibitor for carbon steel in dilute H_2SO_4, J. Fail. Anal. Prev. 21 (2021) 1264–1273.
[42] V. Adinarayanan, P.P. Kumari, S. A Rao, Electrochemical and quantum chemical study to assess the role of (2E)-2-(Furan-2-ylmethylidene) hydrazine carbothioamide as inhibitor for acid corrosion of mild steel, J. Appl. Electrochem. 52 (3) (2022) 627–638.
[43] N. Prithvi, P.P. Kumari, S. A Rao, Inhibitive, Effect of 2-[4-(Dimethylamino) Benzylidene] hydrazinecarbothioamide on corrosion of mild steel in acidic solution, Surf. Eng. Appl. Electrochem. 55 (4) (2019) 481–491.
[44] K. Muthamma, P.P. Kumari, M. Lavanya, S.A. Rao, Corrosion inhibition of mild steel in acidic media by N-[(3,4-Dimethoxyphenyl)Methyleneamino]-4-Hydroxy-Benzamide, J. Bio- Tribo-Corros. 7 (10) (2021).
[45] M. Yadav, D. Behera, S. Kumar, Experimental and theoretical investigation on adsorption and corrosion inhibition properties of imidazopyridine derivatives on mild steel in hydrochloric acid solution, Surf. Interface Anal. 46 (2014) 640–652.
[46] I. Danaee, O. Ghasemi, G. Rashed, M.R. Avei, M. Maddahy, Effect of hydroxyl group position on adsorption behavior and corrosion inhibition of hydroxybenzaldehyde Schiff bases: electrochemical and quantum calculations, J. Mol. Struct. 1035 (2013) 247–259.
[47] F. El-Hajjaji, M. Messali, A. Aljuhani, M. Aouad, B. Hammouti, M. Belghiti, D. Chauhan, M. Quraishi, Pyridazinium-based ionic liquids as novel and green corrosion inhibitors of carbon steel in acid medium: electrochemical and molecular dynamics simulation studies, J. Mol. Liq. 249 (2018) 997–1008.
[48] R. Kumar, S. Chahal, S. Kumar, S. Lata, H. Lgaz, R. Salghi, S. Jodeh, Corrosion inhibition performance of chromone-3-acrylic acid derivatives for low alloy steel with theoretical modeling and experimental aspects, J. Mol. Liq. 243 (2017) 439–450.
[49] S. Deng, X. Li, X. Xie, Hydroxymethyl urea and 1, 3-bis (hydroxymethyl) urea as corrosion inhibitors for steel in HCl solution, Corrosion Sci. 80 (2014) 276–289.
[50] N. Kovačević, A. Kokalj, Analysis of molecular electronic structure of imidazole-and benzimidazole-based inhibitors: a simple recipe for qualitative estimation of chemical hardness, Corrosion Sci. 53 (2011) 909–921.
[51] A. Kokalj, Is the analysis of molecular electronic structure of corrosion inhibitors sufficient to predict the trend of their inhibition performance, Electrochim. Acta 56 (2010) 745–755.
[52] H. Lgaz, R. Salghi, K.S. Bhat, A. Chaouiki, K. Shubhalaxmi, S. Jodeh, Correlated experimental and theoretical study on inhibition behavior of novel quinoline derivatives for the corrosion of mild steel in hydrochloric acid solution, J. Mol. Liq. 244 (2017) 154–168.
[53] J. Haque, V. Srivastava, C. Verma, H. Lgaz, R. Salghi, M.A. Quraishi, N. N-Methyl-N, Ntrioctylammonium chloride as a novel and green corrosion inhibitor for mild steel in an acid chloride medium: electrochemical, DFT and MD studies, New J. Chem. 41 (2017) 13647–13662.
[54] N.O. Eddy, U.J. Ibok, E.E. Ebenso, A. El Nemr, H.E. El Ashry, Quantum chemical study of the inhibition of the corrosion of mild steel in H2SO4 by some antibiotics, J. Mol. Model. 15 (2009) 1085–1092.
[55] M.A. Mumit, T.K. Pal, M.A. Alam, M.A.A.A.A. Islam, S. Paul, M.C. Sheikh, DFT studies on vibrational and electronic spectra, HOMO–LUMO, MEP, HOMA, NBO and molecular docking analysis of benzyl-3-N-(2, 4, 5-trimethoxyphenylmethylene) hydrazinecarbodithioate, Mol. Struct. 1220 (2020), 128715.
[56] N.K. Nkungli, J.N. Ghogomu, Theoretical analysis of the binding of iron (III) protoporphyrin IX to 4-methoxyacetophenone thiosemicarbazone via DFT-D3, MEP, QTAIM, NCI, ELF, and LOL studies, J. Mol. Model. 23 (7) (2017) 1–20.
[57] J.C. Mishma, V.B. Jothy, S. Muthu, A. Irfan, Bonding nature, nucleophilic reactivity and electron excitation of NLO active 2, 6 Dichloroindophenol sodium salt (polar and Non polar solvents) with Topology analysis-Bacterial pathogens study, J. Mol. Liq. 367 (2022), 120533.
[58] R. Soliva, F.J. Luque, M. Orozco, Reliability of MEP and MEP-derived properties computed from DFT methods for molecules containing P, S and CL, Theor. Chem. Acc. 98 (1) (1997) 42–49.
[59] J.A.R. Aslamb, S.H. Alrefaeea, M. Mobinb, A. Aslamc, M. Parveenc, C. M Hussain, Gravimetric,electrochemical, andmorphologicalstudiesofanisoxazolederivativeascorrosioninhibitorformildsteelin1MHCl Arabian J. chem. 13 (2020) 7744–7758.
[60] Y. Zhou, L. Guo, S. Zhang, B. Xiang, Corrosion control of mild steel in 0.1 M H_2SO_4 solution by benzimidazole and its derivatives: an experimental and theoretical study, RSC Adv. 7 (2017), 23961.
[61] J.B. Ekerete, A.O. Odiongenyi, K.E. Essien, E.J. Abai, N.O. Eddy, O. Ekpenyong ngesitIdo, O.E. Oko, Corrosion inhibition potential of two isoxazole derivatives: experimental and Theoretical Analyses, J. Mater. Environ. Sci. 13 (8) (2022) 928–944.
[62] H. Rahmani, F. El-Hajjaji, A. El Hallaoui, M. Taleb, Z. Rais, M. El Azzouzi, B. Labriti, K. Ismaily Alaoui, B. Hammouti, Experimental, quantum chemical studies of oxazole derivatives as corrosion inhibitors on mild steel in molar hydrochloric acid medium,", Int. J. Corros. Scale Inhib 7 (2018) 509–527.
[63] A. Benzai, F. Derridj, O. Mouadili, M. El Azzouzi, M. Kaddouri, K. Cherrak, R. Touzani, A. Aouniti, B. Hammouti, R. Elatki, H. Doucet, Anti-corrosive properties and quantum chemical studies of (Benzoxazol) derivatives on mild steel in HCl (1 M), Portugaliae Electrochem Acta 39 (2021) 135–153.
[64] N. Anusuya, P. Sounthari, J. Saranya, K. Parameswari, S. Chitra, Quantum chemical study on the corrosion inhibition property of some heterocyclic azole derivatives, Orient, J. Chem. 31 (2015) 1741.
[65] B.P. Markhali, R. Naderi, M. Sayebani, M. Mahdavian, Corrosion inhibition of some azole derivatives on carbon steel in hydrochloric acid solution, Anti-Corros. Methods Mater. 61 (2014) 300.
[66] S. El Arrouji, K.I. Alaoui, A. Zerrouki, S. El Kadiri, R. Touzani, Z. Rais, M.F. Baba, M. Taleb, A. Chetouani, A. Aouniti, J. Mater. Environ. Sci. 7 (2016) 299.
[67] A. Guendouz, N. Missoum, A. Chetouani, S.S. Al-Deyab, B.B. Cheikhe, N. Boussalah, B. Hammouti, M. Taleb, A. Aouniti, The influence of some pyrazole derivatives on the corrosion behaviour of mild steel in 1M HCl solution, Int. J. Electrochem. Sci. 8 (8) (2013) 4305.
[68] S. Kumar, V. Kalia, M. Goyal, Newly synthesized oxadiazole derivatives as corrosion inhibitors for mild steel in acidic medium: experimental and theoretical approaches, J. Mol. Liq. 357 (7) (2022), 119077.
[69] D. Yang, X. Feng, N. Yan, Y. Wang, L. Lu, P. Mei, W. Chen, L. Lai, Corrosion inhibition studies of benzoxazole derivates for N80 Steel in 1 M HCl Solution: synthesis, experimental, and DTF Studies, Open Journal of Yangtze Oil and Gas 7 (2022) 101–123, https://doi.org/10.4236/ojogas.2022.72007.
[70] K. Maithili, P. Shetty, P. Preethi Kumari, S. Kagatikar, Mannich base as an efficient corrosion inhibitor of AA6061 in 0.5 M HCl: electrochemical, surface morphological and theoretical Investigations, Arab, J. Sci. Eng. 47 (2022) 7053–7067.